

cMUTs and electronics for 2D and 3D imaging: Monolithic integration, in-handle chip sets and system implications

Chris Daft,* Paul Wagner, Brett Bymaster, Satchi Panda, Kirti Patel and Igal Ladabaum
Siemens Medical Solutions, 1230 Shorebird Way, Mountain View, CA 94039.

Abstract—Capacitive microfabricated ultrasound transducers (cMUTs) have been shown to be practical for medical imaging. Breakthrough performance requires combining these MEMS transducers with electronics. This paper explores synergies between cMUTs and electronics for 2D and 3D imaging. For example, low-noise receive signal conditioning improves tissue penetration, while transmitters capable of arbitrary waveforms minimize clutter. Bias control circuitry can create simple multi-row arrays for improved 2D contrast resolution. It also can enable 3D scanning with less complexity than current alternatives. Matrix transducer elements for 3D present challenges due to their high impedance, number and density. Monolithically integrated cMUTs can offer unique solutions to these problems, enabling isotropic 3D imaging from fully sampled arrays.

I. INTRODUCTION

In recent years the capacitive microfabricated ultrasound transducer (cMUT) has undergone intensive development and created interest as an alternative to ceramic-based ultrasonic probes. An often-quoted advantage of MEMS transducers is their ability to integrate easily with microelectronics. This paper reviews developments in the electronics surrounding the cMUT, and the prospects for creating clinical value with integrated probes. It also presents new results illustrating performance in 2D and 3D imaging for cMUT transducers with electronics at, or close to, the scan-head.

The structure of the paper is as follows: to begin, we present a review of previous work in cMUT imaging and integrated electronics. This covers fabrication methods and linear, convex and contrast-harmonic images. Then we describe electronics for 2D imaging, and 3D bias control scanning. Information on matrix arrays follows, and we conclude with discussion of how cMUTs fit into the future of medical ultrasound.

Probes for 2D imaging do not require monolithic integration, since it is sufficient, and more economical, to locate signal conditioning electronics in the handle. Within the probe handle, amplification (and time-gain

control) remove the signal-to-noise ratio loss from driving a low-impedance cable. Careful attention to transmit-receive switching and other system issues can create a probe which is pin-compatible with the installed base of ultrasound systems. Results from a high-precision ASIC meeting these design goals are described.

All-electronic 3D imaging using bias control is a unique cMUT capability. New *in-vivo* 3D data are presented that were acquired with a simple Fresnel focusing scheme. Bias voltages create scanned elevation beams, while the imager scans normally in the azimuth direction. This approach integrates easily with contemporary imagers, and has important resolution advantages stemming from its ability to create multiple focal zones in range.

Matrix transducers are a major advance over mechanically rocking probes in their image quality and acquisition speed. Monolithic integration benefits cMUT matrix elements greatly because it enables preamplification before any interconnect is traversed. We discuss interconnect and point-spread function issues related to 3D imaging, as well as alternatives to monolithic integration, such as through-wafer vias and flip-chip interconnect.

Lastly, we evaluate the system implications of different ways of making arrays for volumetric imaging. Ultrasound is experiencing severe and increasing competition from improvements in other imaging modalities. cMUTs are positioned to enable a disruptive change in overall clinical workflow, enabled by electronics at the transducer element.

II. FABRICATION OF CMUTS AND ELECTRONICS

We begin by reviewing representative cMUT processes, and examine methods for integrating electronics and addressing the clinical application space. Device electrical data is presented to explain demands placed on the front-end electronics.

Fabrication methods

Several methods to build cMUTs have been described, e.g. [1], [2]. In [3], seven thin film depositions and seven

* Corresponding author's email: daft@ieee.org

lithographic steps are used. The device is fabricated on the top of a silicon substrate with a thermal oxide layer. Chromium electrodes are patterned on a metal layer deposited over this oxide. The electrodes are subsequently protected by a thin film of plasma-enhanced, chemical vapor deposited (PECVD) silicon nitride. To create a releasable membrane, a chromium sacrificial layer is evaporated onto the silicon nitride. This layer is then photolithographically patterned into small circular islands, defining the cavities. A 400 nm PECVD silicon nitride film is deposited over the entire substrate at 350 °C using silane, ammonia, and nitrogen diluted in helium. It produces a conformal film with 100% step coverage. Vias are created by dry etching, and the membranes are released by wet etching through these holes. The holes are then sealed with nitride to avoid ingress of moisture or coupling gel. Finally, an aluminum layer is sputtered on top of the membranes and patterned to define the upper circular electrodes and interconnections between adjacent cells.

Most cMUTs have been made with surface micromachining, where features are built up layer by layer on the surface of a substrate. Recently a bulk micromachined process has been introduced [4]. In this approach, 3D features are etched into the bulk of the material [5]. This process uses silicon-on-insulator (SOI) wafers and creates a membrane of single-crystal silicon. Two wafers are bonded together in a vacuum at 1100 °C and subsequently annealed. One wafer contains the cavity while the other is later etched back to become the membrane. The center frequency is reported to be more uniform than with CVD nitride membranes. Unfortunately, the high temperatures required preclude any integration of electronics with the device.

Methods for integrating electronics

Two methods have been published extending these cMUT manufacturing techniques to allow for integrated electronics. Eccardt and Neiderer [6] created their devices concurrently with the electronics of a BiCMOS process. Only the standard IC layers were used to build the transducers, which constrains the MEMS parameter choices somewhat. The layer heights are fixed by the semiconductor processing, making it necessary to engineer “bumps” into the membrane in order to create the desired vacuum gap. Shift registers were integrated to make transmit delays, and receive preamplifiers were also fabricated with the cMUTs. In this approach the electronics and transducers compete for the same die area, which may limit the sophistication of the electronics and signal-to-noise ratio (SNR). Noble *et al.* [7] sought low-parasitic connectivity to 2D cMUT elements with independent control of design, fabrication and performance of the cMUT and its electronics. Their surface process

contrasts with the through-wafer via design discussed in section VII. PECVD nitride membranes were used with a polyimide sacrificial layer. After plotting stress and stress gradient *vs.* RF deposition power, the authors felt they achieved tight process control at low temperature—for example, thickness control of the Si₃N₄ was better than 1%. In this process the electronics integration required only one extra masking step to gain access through the passivation from the cMUT metal to the ASIC underneath. A charge amplifier with 10 nV·Hz^{-1/2} noise spectral density was integrated with the cMUTs. Total capacitive loading of the cMUT was 0.15 pF, which is sufficiently low to support matrix elements. Our approach to integration also involves post-processing of finished electronics, and is described in section VII.

Practical probes: packaging and electrical performance

After the silicon has been micromachined, several steps remain to produce a finished probe. Mills and Smith [8, 9] describe a typical packaging protocol. In their work the pads on the silicon die link to circuit boards through a high-density-interconnect flex circuit. Parylene is applied for sealing, and then a lens and matched backing are attached. The backing [10] eliminates problems with sound emitted into the silicon bulk; while far less sound is created in this direction than with a PZT resonator, the frequency response is improved with a backing. Leakage and hi-pot testing complete the preparation of a clinically usable device.

In order to understand the demands placed on the electronics surrounding the cMUT, we now discuss the bandwidth and impedance of the transducer itself. Since curved probes represent around 50% of the overall market, a curved transducer is used as an example. Given the strictly planar nature of the IC industry upon whose work cMUTs depend, there was some initial skepticism as to whether cMUTs could address the whole spectrum of clinical applications. We developed a process [11] for making curved arrays and demonstrated it with a 3.5 MHz device with 40 mm radius of curvature (ROC). An analytical model of the stress added to the membrane by substrate bending drove the mechanical design parameters. With the array pictured in Figure 1, we found little change in the membranes’ air resonances after curvature. Air resonance is a sensitive indicator of imaging performance that provides excellent feedback on device behavior immediately after wafer fabrication, and prior to all post-fab processing. The assembly process was carefully designed to minimize stress build-up during packaging and to create accurate curvature. Standard semiconductor thinning methods such as etching, polishing and lapping are used in the process. Measured tolerance of the ROC

was $\pm 10 \mu\text{m}$, and probe fractional bandwidth (half-power, one-way) was 125%.



Figure 1: A 3.5 MHz curved cMUT array with 128 elements and 40 mm radius of curvature.

Origin of electronic performance requirements

Typical measurements of impulse response and power spectrum for this type of array are given in Figure 2 and Figure 3.

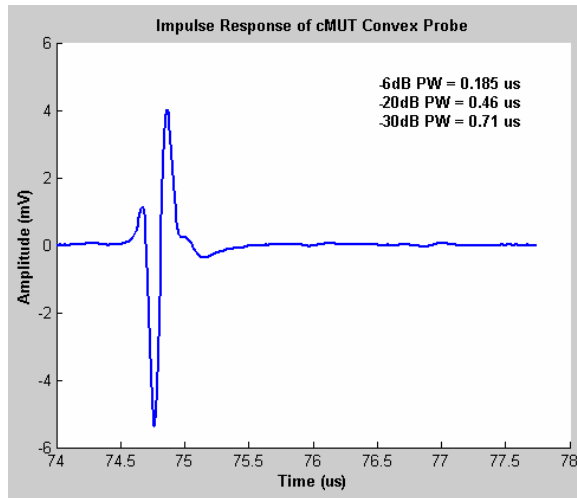


Figure 2: Measured impulse response of curved array. Note compact length and absence of ring-down.

The smooth frequency response contrasts with typical ceramic and single crystal piezoelectrics, which have more boxcar-shaped power spectra and longer impulse responses resulting from their many poles. The resonance of cMUTs is over-damped by the fluid loading. In mid-band, the

membrane impedance is small enough that the impedance seen by the transmitter is the parallel combination of the plate reactance $(j\omega C)^{-1}$ and the transformed mechanical load impedance, $Z_A A / (EC)^2$. Here Z_A is the acoustic load impedance (which tends to 1.5 Mrayl for elements wider than a wavelength, and is reactive for smaller elements), C is the element capacitance, A is the element area and E is the electric field in the gap. Therefore, large fields yield smaller radiation impedances seen from the electrical side, with reduced shunting by the plate capacitance. This simplifies drive circuitry and increases bandwidth. It is clear from these graphs that receive electronics needs broad bandwidth and linear phase response to preserve the cMUT's image quality.

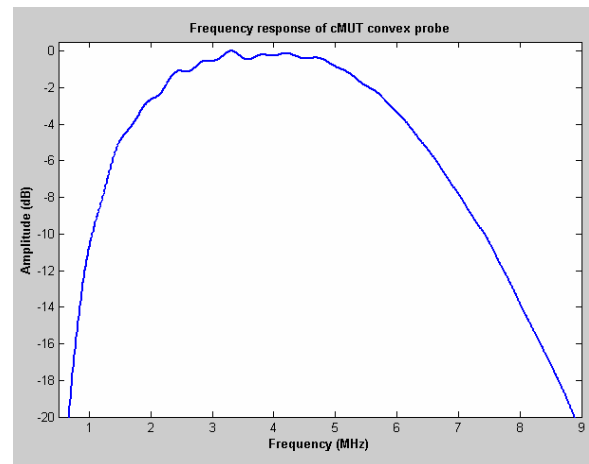


Figure 3: Measured frequency response of curved array. The slow decrease away from the center frequency is advantageous for coded excitation.

Impedance differences from PZT

Another important consideration for both transmit and receive electronics is the difference in impedance magnitude between PZT and cMUT elements of the same area. While the plate separation in a cMUT is roughly 200 times smaller than typical PZT thickness, the relative permittivity (ϵ_R) of PZT is 1500-3000; the effective ϵ_R for a cMUT is between 1 and 7, depending on its construction. Thus typical cMUTs have ~ 3 times higher impedance than PZT-5H elements of the same dimensions. This motivates receive electronics close to the element, so as to avoid SNR loss from driving ~ 200 pF of cable and system capacitance.

III. 2D CLINICAL IMAGES

In this section we examine how these electrical characteristics influence clinical images, and describe electronics used to create them.

cMUT Imaging in the literature

Mills and Smith [8, 9] showed improved axial resolution in carotid artery images. They observed 132% fractional bandwidth from bulk micromachined cMUTs. Scans were shown with normal biasing, and also with the membrane biased beyond collapse. In their data, operating in collapse mode did not seem to improve sensitivity; they also note that long-term reliability of collapse mode has not been investigated in detail. Suggested applications for cMUT arrays modeled on existing designs include micro-calcifications in the breast, small thyroid abnormalities, and delineation of intimal linings in vessels where evidence of plaque build-up is sought.

Some representative 2D images with transformers

Figure 4 (small parts), Figure 5 (breast) and Figure 6 (musculoskeletal) illustrate how the compact impulse response translates into better image quality using a 9 MHz linear array with 0.2 mm pitch. Rounding out this brief survey, we then present curvilinear abdominal and harmonic images.

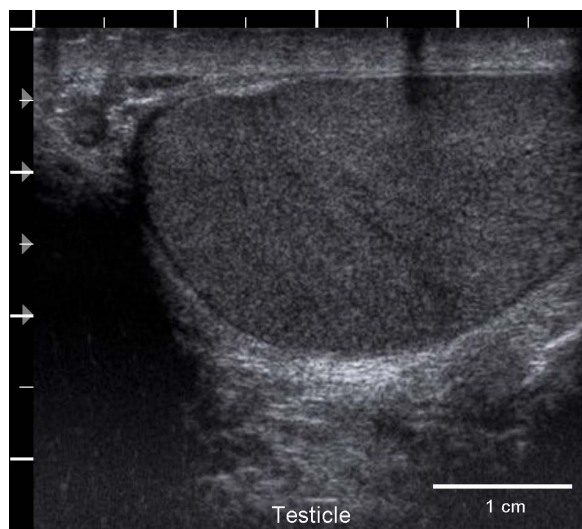


Figure 4: Testicle imaged at 9 MHz with a 192-element, linear array. Note resolution of the testicular capsule and scrotum as well as delineation of the tiny vessels.

The in-handle electronics used here was very simple: each channel had a transformer for impedance matching to the cable, as well as a resistor-capacitor network for biasing the micromachined drums. The transformer makes the higher-impedance cMUT efficient for a standard ultrasound transmitter to drive. However, while power transfer on receive is adequate, the preamplifier in the system makes more noise than the intrinsic cMUT noise

when the voltage is stepped down by the transformer (see section IV). The overall noise figure is sub-optimal, and penetration is limited.



Figure 5: Breast scan with the same array. Contrast differentiation between fat, glandular, and muscle layers is evident. Cooper's ligament is resolved.

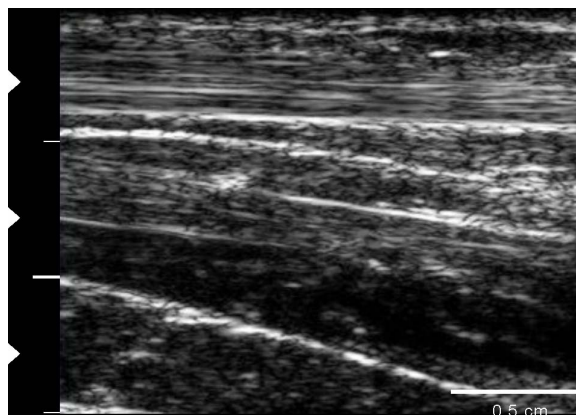


Figure 6: Forearm tendon imaged with the same array. Note the clearly resolved horizontal structures and the definition within the tendon.

Figure 7 shows an abdominal view from the 3.5 MHz curved array described in section II. The 64-channel imager used here curtails the aperture in the far field, limiting the lateral resolution to some extent.



Figure 7: Abdominal image showing liver and diaphragm, taken with a 3.5 MHz curved array and a 64-channel imager. The inset shows the surprising pliability of the thinned silicon die.

The contrast-enhanced harmonic image in Figure 8 was obtained with a lower-frequency linear cMUT array in order to effectively excite the agent. In this case the low-Mechanical Index (MI) mode was used with pulse inversion detection of the harmonics. The large echogenic circular structure is the carcinoma.

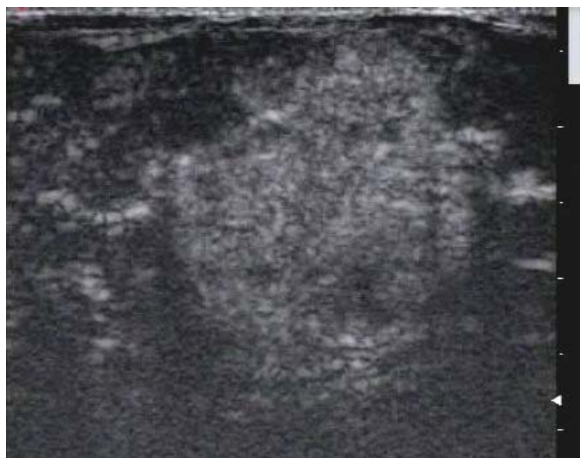


Figure 8: Harmonic image of a malignant ductal infiltrating carcinoma in the breast. The contrast agent is *Sonovue*® SF₆ (Bracco, Geneva). A 192-channel linear array transmitted at 2.4 MHz.

With these images as a baseline, we now describe electronics that offers further image quality improvement.

IV. ELECTRONICS FOR 2D IMAGING

To achieve the full potential of the cMUT, we must locate electronics near the transducer element itself. Electronic requirements for 2D imaging, solutions and their implications are described in this section.

Receiver electronics needs for cMUTs

Connecting a cMUT directly to a cable has SNR consequences that are straightforward to evaluate if the system terminates the cable with a matched resistive load (as some do) and the system preamplifier noise is larger than the cMUT's intrinsic noise as it appears at the preamp input (usually the case). We further assume negligible cable losses for simplicity. Then direct connection results in a voltage division $R_L/(R_L+R_M+jX_M)$ where R_L is the cable impedance and (R_M+jX_M) is the cMUT impedance. For a 75 Ω cable and a cMUT impedance of (100-j500) Ω, this causes a 17 dB reduction in receive SNR—far from optimal for penetration. If we introduce a transformer (as was done for the preceding images) and choose a turns ratio of 2.6:1, equalizing the cMUT impedance magnitude with the cable, the SNR degradation becomes the combination of the voltage step-down of the transformer (8 dB in this example) and the voltage division, which is a further 4 dB. Adding a transformer consequently reduces the receive SNR loss from 17 dB to 12 dB.

To improve this situation we must create a preamplifier with a gain large enough to overwhelm the noise of the first system amplifier, and locate it before the cable. This circuit should load the cMUT as little as possible and have an output impedance appropriate for the cable load. Given sufficient gain, the overall noise figure will then be approximately that of this initial amplifier.

Position of receive amplifier

While it is practical to build cMUTs with the amplifier on the same wafer, this is not the most economical choice for 2D imaging. Attaching an array element to a circuit board via a flex circuit causes little SNR loss if the interconnect is designed carefully. This means that traditional IC packages can be used and the cMUTs are built on blank wafers. The flex circuit, PCB and IC package parasitics can be held to around 10 pF. This causes an 0.5 dB SNR penalty for a 4 MHz array, rising to 1 dB for a 10 MHz probe. Figure 9 is a block diagram of a multi-chip-module approach that enhances the SNR as well as dealing with transmit-receive switching.

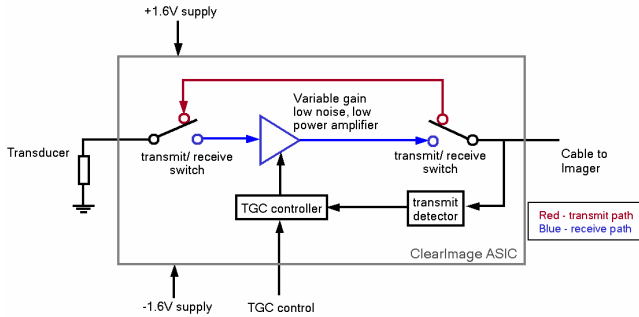


Figure 9: In-handle electronics for penetration improvement in 1D cMUT arrays.

In this setup the transmit-receive switching requires low “on” resistance to avoid adding to the receiver noise figure, and also to minimize power dissipation during the transmit pulse. The preamplifier noise figure must be as low as possible given power constraints in the probe handle. Its gain begins at a low value and increases as the sound pulse travels deeper in the tissue. This time-gain control (TGC) allows for large signal handling without excessive distortion early in the beam, as well as providing enough gain for optimal overall system SNR later on. In our implementation we measured 2nd harmonic distortion products below -68 dB at maximum signal, while maintaining a 4 dB overall noise figure at maximum gain with a cMUT connected. Some intelligence was added to the ASIC so significant power was consumed only when necessary. Inactive channels can be swiftly put in a “sleep” mode, while a variable-power feature reduces power for conditions when the best SNR is not required. For widest applicability, this system should be pin-compatible with the installed base of imagers. To that end, the transmit detection is automatic.

Measurement of SNR gain

Using a 3.5 MHz center-frequency abdominal cMUT, we compared the receive SNR of the arrangement of Figure 9 with a cMUT with no amplification. The imager front-end was typical of contemporary designs. Figure 10 shows the results as a function of frequency. The moderate frequency dependence stems from the variation in cMUT impedance interacting with the amplifier’s noise current. These results show that significant penetration improvement is possible with receive processing electronics in the probe handle.

Transmit electronics needs for cMUTs

cMUT transmit electronics requirements are defined by the need to achieve large pressures within the limits imposed by the FDA 510(k) regulations. It was suggested early on that cMUTs would have difficulty with harmonic imaging

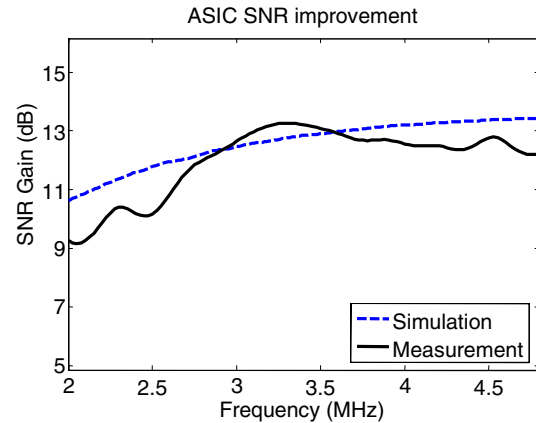


Figure 10: Comparison of measured and simulated SNR improvement for an abdominal cMUT. SNR gain over a cMUT with no electronics is plotted.

due to the non-linear transfer function relating applied voltage to output pressure. When driving cMUTs to produce output pressures at the regulatory limits, second harmonic at roughly -20 dB is created with typical designs. This creates clutter in a harmonic image, which can be removed in several ways. One solution uses harmonic-only transmit events [12]. Hossack *et al.* [13] presented an approach in which the linearized transfer function and measurements of the harmonic output are used to iteratively create a pre-distorted transmit signal. They note a reduction in harmonic generation of between 18-20 dB. Modern transmitters in ultrasound imagers are capable of the waveform fidelity needed by this technique.

Coded excitation is especially useful for increasing the penetration depth for cMUTs while adhering to regulatory pressure maxima. This is due to an increase in the gain-bandwidth product derived from both large raw device bandwidth and the smoother frequency response. Chiao and Hao [14] have reviewed methods for transmit waveform coding. Overall, transmitter circuitry demands for coded excitation with cMUTs are similar to those of their piezoelectric brethren. In cases where the transmit amplitude of an existing system is limited, a transformer in the probe handle can be helpful.

V. 3D IMAGING WITH BIAS CONTROL

The numerous barriers to 3D imaging have been studied since the dawn of the field of ultrasound, but only in the past four years have noticeable clinical inroads been achieved by commercial 3D imaging systems. An all-electronic cMUT alternative to commercially available rocking probes is presented in this section, after a brief review of the state of the art.

Contemporary 3D imaging

Progress in imaging with a matrix of elements has been paced by practical considerations, such as how to connect several thousand high-impedance PZT elements through a thick backing. No feasible cabling can connect this quantity of transmit and receive signals to the imager. Data compression *via* partial receive beamforming from this “acoustic retina” is possible prior to the cable, but the per-channel power that can be expended within the handle is severely limited. A fundamental, clinically-driven requirement is simply that there is no more time available to acquire a 3D volume than a 2D slice, due to physiological motion. This demands two orders of magnitude of acceleration in data collection. If a 2D scan occurs at 10 frames per second (typical for General Imaging if there is no flow measurement) acquiring one volume with the same sampling will take 10 seconds. While there are tricks to accelerate this slightly, and schemes to correlate elevation slices with tissue motion, acquisition remains too slow.

Obstetrical 3D ultrasound has created a great deal of press recently, using the rocking 1D array technique first described by Kirbach *et al.* [15]. Several probes are available from various manufacturers based on this idea. Difficulties with this approach include the lack of dynamic or zone-based focusing and aperture control in elevation. A fixed elevation lens compromises resolution away from its focus. Simultaneous receive beams can be formed only in azimuth (not elevation) which limits the acquisition rate. Rapid motion of the probe impairs flow detection, and mechanical complexity reduces reliability compared to solid-state probes.

Bias controlled imaging concept

3D imaging using bias control is a unique cMUT capability. Here the physical basis is reviewed, and then 3D images acquired with this simple electronic scanning scheme are presented. In [12] the idea of altering the bias voltage to create a better focus in elevation was introduced. The polarity of the output pressure inverts if the sign of the bias voltage is changed while the transmit pulse remains constant. An equivalent circuit [16] for the cMUT explains this effect. It includes an electrical to mechanical transformer whose turns ratio n is proportional to the DC bias voltage: $n=EC$, where E is the electric field in the gap and C is the plate capacitance. The turns ratio and in-circuit element transduction efficiency changes sign and magnitude with gap field.

In a surface micromachined cMUT, a patterned metallization defines the azimuth elements on one side of the device; traditionally the other side has been a continuous ground electrode. This ground electrode can be

replaced with “bias lines” orthogonal to the azimuth elements. This allows a given azimuth element to have a bias voltage that varies in elevation without disturbing the imager's azimuth focusing. A pattern of bias voltages can be used as a Fresnel lens to focus in elevation. We can then make an array that looks one-dimensional to the imager while creating a movable focus in the orthogonal direction. This side-steps one of the most difficult issues with 2D transducer matrices: for a fully-sampled aperture there must be, at a minimum, several thousand elements, each of which has a high impedance and requires a separate delay and summation for beamforming. If there are N azimuth elements and M bias lines, only $(N+M)$ interconnects are required for this type of probe, rather than NM interconnects in a traditional 2D matrix. One transducer of this type we built had $N=192$ and $M=280$, so the interconnect complexity was decreased by a factor of 114. As well as focusing at a specified depth, the aperture can effectively be apodized. That is accomplished by removing the bias voltage, which decreases the element efficiency so markedly that the bias line can be assumed to be “off”. Elevation aperture translation is achieved in a linear format. The edges of the probe's active aperture can be windowed by decreasing the magnitude of their biasing.

Transmitted harmonic cancellation

Bias line manipulation can also cancel unwanted harmonic output. The phase of the even harmonics in the transmitted pressure do not vary with bias sign, while the fundamental (and odd harmonics) do. This means an alternating bias pattern at the maximum spatial frequency produces only even harmonics when the cMUT is driven into significant nonlinearity. We can use this to cancel harmonics at any drive level with a simple three-firing scheme. Consider transmitting the two signals used in standard pulse inversion harmonic imaging $p(+V_{AC})$ and $p(-V_{AC})$, and coherently summing the received signal. Then transmit $p(AltBias)$, a signal with the alternating bias pattern and subtract twice its received signal:

$$Image = p(+V_{AC}) + p(-V_{AC}) - 2 \cdot p(AltBias)$$

The result of this pulse sequence is complete cancellation, in time and space, of the harmonics generated by the cMUT. It works with any transmit signal—in particular, no pre-distortion of the transmit voltage is necessary.

Figure 11 shows a practical implementation of the bias scanning idea in a high-frequency probe designed for applications such as breast imaging. The imager performs its normal scanning in the azimuth direction (horizontal in Figure 11) while the bias lines are scanned vertically. This type of scan format is already supported by most premium imagers.

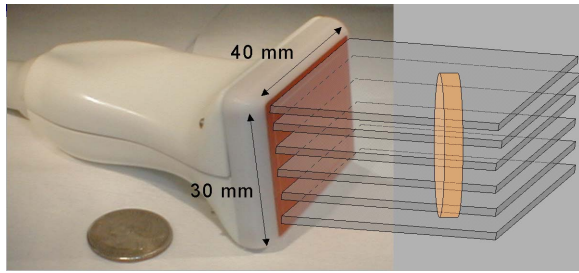


Figure 11: 3D linear scanning via bias-line control. The array scans horizontally using the system beamformer, and vertically by manipulating the bias pattern.

Figure 12 shows a coronal view, or C-scan, resolution test of the above probe using a coin. In the top two images the surface of the coin is pictured, while the lower two have the C-scan plane positioned so that only the uppermost features of the coin, such as the rim, are resolved. Azimuth is horizontal and elevation is vertical in this figure. Two scanning approaches are used: on the left-hand side a fixed, unipolar aperture is translated across the coin, while on the right the Fresnel focusing is turned on. A significant improvement in elevation resolution is observed.

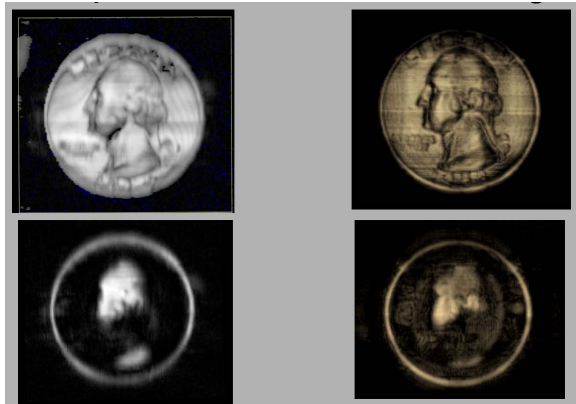


Figure 12: Effect of Fresnel focusing on resolution, visualized using a coin. The left-hand side images use bias only for aperture translation, while the right-hand side images incorporate Fresnel focusing.

In a scan with multiple transmit focal zones, the elevation focal depth can be adjusted for each zone, exactly as in azimuth transmission. Receive elevation focusing matches the zone depth. Since there is no probe motion involved in scanning, flow detection is accurate. In this simplest incarnation the bias scanned transducer cannot perform parallel beam formation in the elevation dimension; the acquisition rate matches rocking 1D arrays.

VI. 3D CLINICAL VOLUME DATA

In this section tissue data are presented using the bias scanning technique. Figure 13's three images show slices through a 3D data set of the foot tendons of a diabetic, taken at 9 MHz.

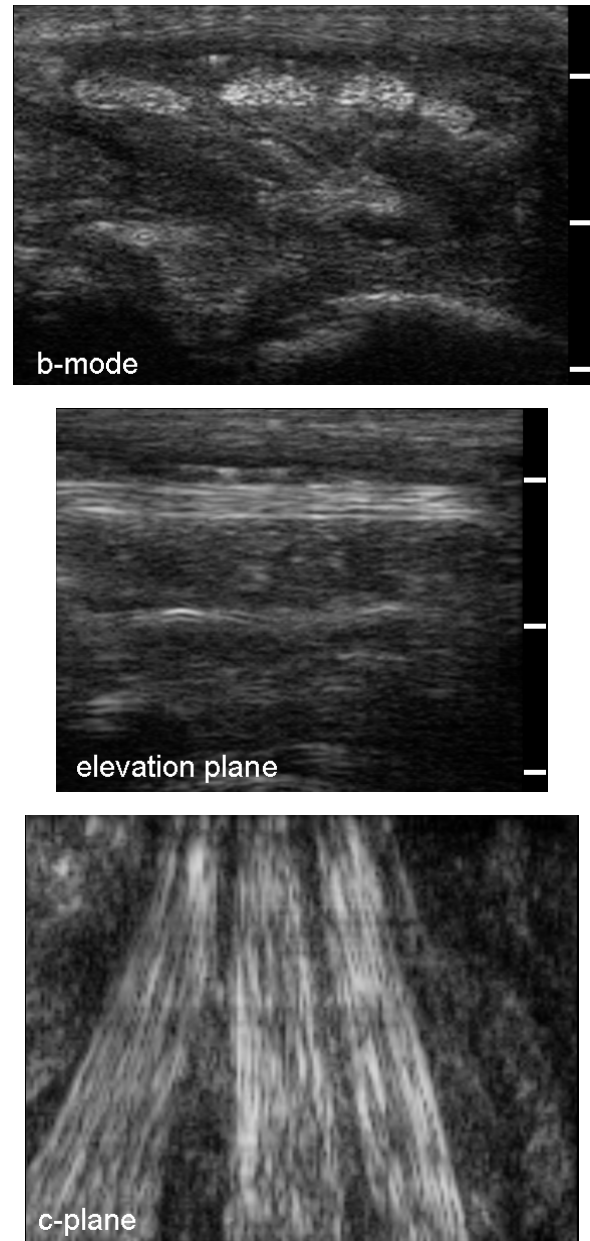


Figure 13: 3D data from bias scanned foot tendons. B-mode and elevation plane images have 3.2 cm depth displayed. The C-plane image is 4x3 cm.

All 3D data processing took place using the 3D Sono-Scan software (TomTec GmbH, Unterschleissheim, Germany). The C-plane image is of particular interest as it is unavailable with a 1D array, no matter how the probe is oriented. In this view the tendons' anatomy is much more clearly apparent than in the azimuth and elevation planes. Figure 14 shows four views of a breast tumor.

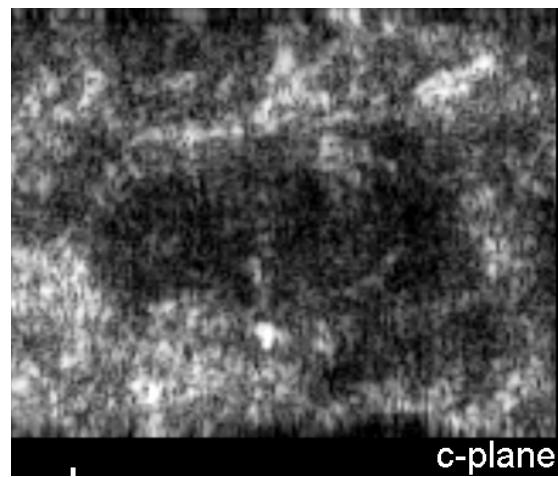
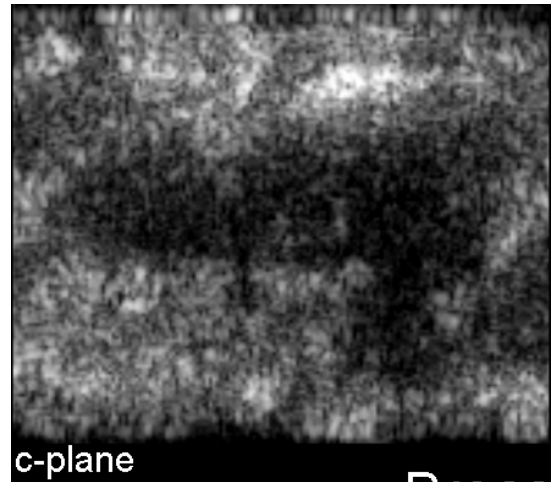
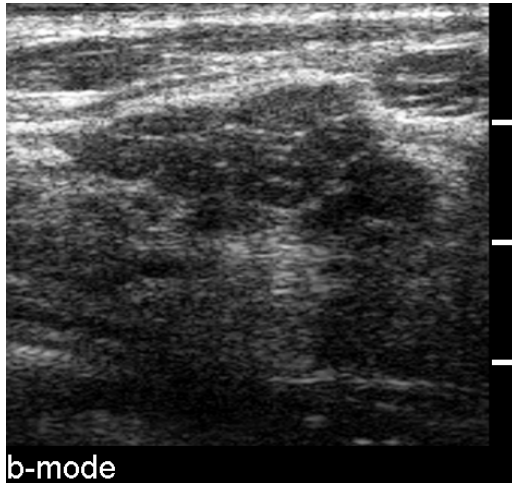


Figure 14: Slice views of a breast mass. B-mode and elevation images have 3.6 cm depth displayed. The C-plane image is 4x3 cm. The C-plane images are in the correct orientation to detect spiculation.

Figure 14's two C-plane images (above) are telling. The physician reviewing these images commented that it was easier to positively identify the structure as a fibroadenoma (a benign, glandular tumor) from the C-planes than the other views. No spiculation was evident in these coronal sections, and the surrounding texture was even. These examples suggest that the bias scanning technique, despite its simplicity, is able to reveal new clinical information.

Malignancy in breast tumors is often indicated by spiculation [17], a pattern of alternating hypoechoic and hyperechoic lines that radiate in several directions from the mass into the surrounding tissue. 2D imaging (which can create the azimuth and elevation slices above) rarely demonstrates spiculation since it is normally oriented parallel to the surface of the skin [18].

VII. 3D IMAGING WITH MATRIX TRANSDUCERS

While mechanically rocking probes can fulfill some needs, the potential of a matrix of elements is much higher. Beams may be steered in any direction, and elevation dynamic focus becomes possible. Parallel receive beam formation in azimuth and elevation are feasible, improving

acquisition rate. We outline the requirements for a successful matrix design and then review cMUT progress towards a practical transducer.

Design parameters for matrix probes

The first matrix transducer was built at Duke University in 1991 [19, 20]. The goals were to create a hand-held transducer without moving parts, capable of rapidly scanning a volume and enabling 3D visualization of dynamic structures. Due to the small number of channels available, they were compelled to use sparse transmit and receive apertures. While Turnbull [21] found that sidelobes are reasonable at element reduction ratios of 4-6, penetration is dependent on array area. With typical regulatory and electronic limitations, a 6th order sparse array will lose 8 dB of transmit power and the received signal will be a further 8 dB noisier. This SNR loss makes such designs difficult to implement clinically.

Fully-sampled designs have been the focus of commercial development. Greenstein *et al.* [22] described the design, fabrication and testing of a 2500-element, 2.5 MHz phased array with 0.25 mm square elements, illustrating the advanced interconnect required. Savord and Solomon [23] developed this into a practical transducer whose elements are partially beamformed in the handle. This makes a probe that has only 128 cables attaching it to the system. A wire frame connects to the sides of the backing block, where ASICs beam-form groups of elements together. The high impedances of both PZT and cMUT matrix elements demand supporting electronics nearby. Analog circuitry is used to perform sub-array delay-and-sum operations within a very tight power budget. Phase shifters, analog RAM, sample-and-holds or CCDs are possible ways to create these delays.

cMUT matrix arrays: die bonding, or micromachining above a finished IC

Oralkan *et al.* [24] have made 3D images with a matrix of surface micromachined cMUTs. Interconnect is achieved by a flip-chip technique with deep reactive-ion etching (DRIE) of through-wafer vias. The die was bonded to a glass carrier chip, to be replaced by an ASIC in the final device. A major issue with the 20:1 aspect ratio vias is parasitic capacitance, both along the walls of the via and at the top and bottom pads. Reverse-biased metal-insulator-semiconductor junctions [25] reduce this on the walls, while *p-n* junctions may help with pad capacitance. A 16x16 array for an endoscope using similar technology has recently been built [26]. A stack of metal layers on the ASIC bond pads forms bumps; these are heat bonded to the cMUT die's back-side aluminum bond pads.

As both the PZT and cMUT examples show, interconnect to the array is crucial. Perhaps the simplest solution to this is to build cMUTs on top of finished wafers. In [27] we described monolithic integration of high-quality imaging cMUTs with analog switching electronics. Figure 15 is a micrograph of cMUTs with underlying CMOS circuitry. Water tank results demonstrated that these transducers, integrated with controlling switches, are fully functional both electronically and acoustically. As with the through-wafer via method, this approach allows separate optimization of the cMUT and the electronics beneath. Preamplification can be achieved with negligible parasitics (even for matrix elements) if the cMUTs are grown on the IC wafer.

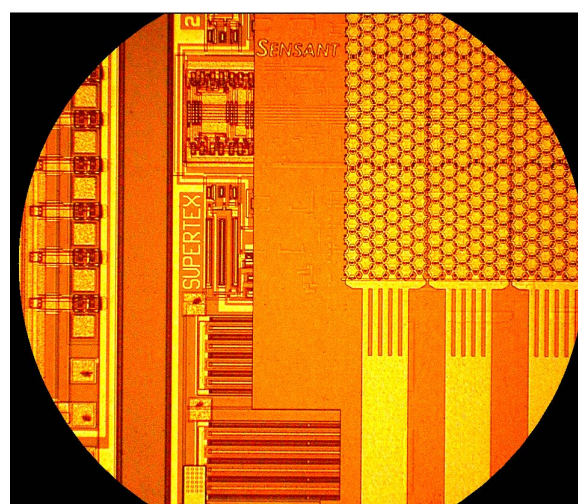


Figure 15: cMUTs built on top of Supertex high-voltage switches. The micromachining was subsequent to the CMOS IC fabrication.

VIII. CONCLUSIONS

This article has reviewed fabrication of cMUTs with electronics, presented 2D images and discussed electronic improvements for 2D imaging. 3D imaging with bias control was introduced as an extension of the Fresnel focusing previously reported, and two cases of *in-vivo* volume data were presented. We have examined work on cMUT matrix transducers and compared to their PZT equivalents. The system implications of these cMUT imaging schemes are fairly modest. In 2D imaging, preamplification is required in the probe handle and a transformer may be useful if the imager's transmit voltage is limited. 3D bias-controlled imaging requires some simple coordination whereby the slice position and focal zone determine the bias pattern to be applied to the array in elevation.

cMUTs and the future of ultrasound

In conclusion, it is worthwhile to explore how more ambitious cMUT and electronics combinations might intersect with clinical needs. For many years, ultrasound has been the most widely used imaging modality. It is non-ionizing and lacks contraindications. The equipment is compact enough to take to the patient, and images are produced in real-time.

Garra [28] notes the erosion of ultrasound's position in radiology, arising from spectacular recent performance gains for CT (a five-fold improvement in patient throughput in the last decade), MR (increased speed, and flow imaging without contrast) and PET-CT (evaluation of metabolism, e.g. for cancer diagnosis). Clinicians already perceived ultrasound images as noisy due to speckle, and the resolution is worsening because of the obesity epidemic. This is true even in applications such as obstetrics. Ultrasound has historically been the dominant modality, but MRI provides far higher image quality for obese patients. Very few new radiologists are choosing ultrasound as a subspecialty at this time.

From the equipment manufacturer's perspective, the answer to this unsettling trend contains both image quality and workflow components. For ultrasound to avoid being relegated to low-cost niche markets, it needs several new characteristics. First, the data must be acquired faster than the 15 minutes required for a complete CT scan—this is rarely the case today. Consequently, there is no time for repeated probe re-positioning to obtain the correctly diagnostic 2D slice orientations. The imaging must be reproducible, operator-independent and easier to accomplish than it is currently. Resolution should be at the diffraction limit in all dimensions, at all depths, with phase aberration automatically corrected and speckle removed or attenuated. The data-set must always contain the diagnostic information the physician will be seeking upon their later review. This mandates 3D imaging. The system should alert the operator if an inadequate acoustic window has been chosen, to avoid later patient recall at all costs. Measurements of tissue volumes and flow rates should exceed those of the other modalities in accuracy. Enough data should be available to enable processing methods such as elasticity imaging, frequency dependence of backscatter and vector flow.

These are severe demands, but the interaction of sound with tissue is extremely rich. Everything necessary to achieve these goals exists at the elements of a 2D array. The challenge is to extract *all* of the information contained in the backscattered wave. It calls for a redefinition of the imaging architecture towards highly parallel acquisition, and advanced processing of channel data prior to beam formation. cMUTs are uniquely positioned to enable

imaging involving high-density electronics situated at the transducer element, so we look forward to many researchers tackling these problems with a new box of tricks.

ACKNOWLEDGMENTS

We are very grateful for assistance from many quarters: Drs. Martegani and Aiani (Valduce Hospital); Paolo Pelegretti and Franco Bertora (Esaote S.p.A.); Lewis Kwok, William Wong, Franklin Gonzalez and Bill Ingram (Supertex); Bernhard Mumm (TomTec); Bill Buchele and Patrick O'Hare (B&A); Steve Barnes and Sean Hansen (Siemens). Sam Calmes, Heman Chu, Andrew Cittadine, Kathy Jackson, Joe Lee, Albert Mique and Keith Wong provided essential support.

REFERENCES

- [1] Jin, X., Ladabaum, I. and Khuri-Yakub, B.T., "The microfabrication of capacitive ultrasonic transducers," *J. Microelectromech. Syst.* **7**(3), 295-302, 1998.
- [2] Jin, X., Ladabaum, I., Degertekin, F.L., Calmes, S. and Khuri-Yakub, B.T., "Fabrication and characterization of surface micromachined capacitive ultrasonic immersion transducers," *J. Microelectromech. Syst.* **8**(1), 100-114, 1999.
- [3] Caliano, G. *et al.*, "A cMUT Linear Array Used as Echographic Probe: Fabrication, Characterization, and Images," in *Proc. 2004 IEEE Ultrasonics Symposium*, 395-398.
- [4] Huang, Y., Ergun, A.S., Haeggstrom, E., Badi, M.H. and Khuri-Yakub, B.T., "Fabricating capacitive micromachined ultrasonic transducers with wafer-bonding technology," *J. Microelectromech. Syst.* **12**(2), 128-137, 2003.
- [5] Madou, M., "Fundamentals of Microfabrication," 217ff. Boca Raton, FL: CRC Press 1997.
- [6] Eccardt, P.-C. and Niederer, K., "Micromachined ultrasound transducers with improved coupling factors from a CMOS compatible process," *Ultrasonics* **38**, 774-780, 2000.
- [7] Noble, R.A. *et al.*, "Low-Temperature Micro-machined cMUTs with Fully-Integrated Analogue Front-End Electronics," in *Proc. 2002 IEEE Ultrasonics Symposium*, 1045-1049.
- [8] Mills, D.M. and Smith, L.S., "Real-time in-vivo imaging with capacitive micromachined ultrasound transducer (cMUT) linear arrays," in *Proc. 2003 IEEE Ultrasonics Symposium*, 568-571.
- [9] Mills, D.M., "Medical Imaging With Capacitive Micromachined Ultrasound Transducer (CMUT) Arrays," in *Proc. 2004 IEEE Ultrasonics Symposium*, 384-390.
- [10] Ladabaum, I., Wagner, P., Zanelli, C., Mould, J., Reynolds, P. and Wojcik, G., "Silicon substrate ringing in microfabricated ultrasonic transducers," in *Proc. 2000 IEEE Ultrasonics Symposium*, 943-946.
- [11] Wong, K.A., Panda, S. and Ladabaum, I., "Curved micromachined ultrasonic transducers," in *Proc. 2003 IEEE Ultrasonics Symposium*, 572-576.
- [12] Daft, C., Wagner, P., Panda, S. and Ladabaum, I., "Elevation beam profile control with bias polarity patterns applied to microfabricated ultrasound transducers," in *Proc. 2003 IEEE Ultrasonics Symposium*, 1578-1581.
- [13] Zhou, S., Reynolds, P. and Hossack, J., "Precompensated excitation waveforms to suppress harmonic generation in MEMS electrostatic transducers," *IEEE Trans. UFFC* **51**(11), 1564-1574, 2004.

- [14] Chiao, R.Y. and Hao, X., "Coded Excitation for Diagnostic Ultrasound: A System Developer's Perspective," *IEEE Trans. UFFC* **52**(2), 160-170, 2005.
- [15] Kirbach, D. and Whittingham, T.A., "3D ultrasound—the Kretztechnik Voluson approach," *Europ. J. Ultrasound* **1**, 85-89, 1994.
- [16] Ladabaum, I., Jin, X., Soh, H.T., Atalar, A. and Khuri-Yakub, B.T., "Surface micromachined capacitive ultrasonic transducers," *IEEE Trans. UFFC* **45**(3), 678-690, 1998.
- [17] Stavros, A.T. *et al.*, "Solid breast nodules: Use of sonography to distinguish between benign and malignant lesions," *Radiology* **196**(1), 123-134, 1995.
- [18] Rotten, D., Levaillant, J. M. and Zerat, L., "Analysis of normal breast tissue and of solid breast masses using three-dimensional ultrasound mammography," *Ultrasound Obstet. Gynecol.*, **14**(2), 114-124, 1999.
- [19] Smith, S.W., Pavy, H.G., Jr. and von Ramm, O.T., "High-speed ultrasound volumetric imaging system. I. Transducer design and beam steering," *IEEE Trans. UFFC* **38**(2), 100-108, 1991.
- [20] von Ramm, O.T., Smith, S.W. and Pavy, H.G., Jr., "High-speed ultrasound volumetric imaging system. II. Parallel processing and image display," *IEEE Trans. UFFC* **38**(2), 109-115, 1991.
- [21] Turnbull, D.H. and Foster, F.S., "Beam steering with pulsed two-dimensional transducer arrays," *IEEE Trans. UFFC* **38**(4), 320-333, 1991.
- [22] Greenstein, M., Lum, P., Yoshida, H. and Seyed-Bolorforosh, M.S., "A 2.5 MHz 2D array with Z-axis electrically conductive backing," *IEEE Trans. UFFC* **44**(5), 970-977, 1997.
- [23] Savord, B. and Solomon, R., "Fully sampled matrix transducer for real time 3D ultrasonic imaging," in *Proc. 2003 IEEE Ultrasonics Symposium*, 945-953.
- [24] Oralkan O., Ergun, A.S., Cheng, C.H., Johnson, J.A., Karaman, M., Lee, T.H. and Khuri-Yakub, B.T., "Volumetric ultrasound imaging using 2-D CMUT arrays," *IEEE Trans. UFFC* **50**(11), 1581-94, 2003.
- [25] Cheng, C.H., Chow, E.M., Jin, X., Ergun, A.S. and Khuri-Yakub, B.T., "An efficient electrical addressing method using through-wafer vias for two-dimensional ultrasonic arrays," in *Proc. 2000 IEEE Ultrasonics Symposium*, 1179-1182.
- [26] Wygant, I.O. *et al.*, "Integrated Ultrasonic Imaging Systems Based on CMUT Arrays: Recent Progress," in *Proc. 2004 IEEE Ultrasonics Symposium*, 391-394.
- [27] Daft, C., Calmes, S., da Graca, D., Patel, K., Wagner, P. and Ladabaum, I., "Microfabricated ultrasonic transducers monolithically integrated with high voltage electronics," in *Proc. 2004 IEEE Ultrasonics Symposium*, 493-496.
- [28] Garra, B.S., "Radiology must change to retain ultrasound role," *Diagnostic Imaging* **27**(6), 27-32, 2005.